RSC Advances

PAPER

View Article Online
View Journal | View Issue

Cite this: *RSC Adv.*, 2026, **16**, 13682

Comparative efficacy of novel mono- and di-azomethine clubbed schiff bases against α-glucosidase and human bacterial pathogens: *in vitro*, molecular docking, and MD simulations

Anee Taj,[a] Iqra Kalsoom,[a] Asma Zaidi,[a] Majid Ali,[ab] Mesaik M. Ahmed,[cd] Atia Masood Ahmed,[e] S. Tasqeeruddin,[f] Mohammad Zubair,[cd] Shamina Begum,[c] Ajmal Khan,*[gh] Syed Majid Bukhari*[a] and Ahmed Al-Harrasi*[g]

A series of new mono-azomethine (compounds **1–10**) and di-azomethine (compounds **11–20**) Schiff bases of 4-aminoantipyrine (compound **1–20**) were synthesized, characterized, and evaluated for α-glucosidase inhibitory activity along with antibacterial potential in parallel to explore their broader pharmacological potential. In terms of antibacterial activity, mono-azomethine derivatives were generally more effective than di-azomethine analogues. In particular, compounds **5** and **6** with –OH substitution on the benzene ring presented excellent inhibition zones (51 ± 0.7 mm and 46 ± 0.5 mm against *Salmonella typhi*; 48 ± 0.6 mm and 43 ± 0.8 mm against *Staphylococcus aureus* respectively). Di-azomethine Schiff bases were found to be less effective as compared to mono-azomethine, presenting zones of inhibition at 38 ± 0.8 mm for compound **13** and 34 ± 0.9 mm for compound **10** against *Staphylococcus aureus*, and compound **19** at 37 ± 0.9 mm against *Salmonella typhi*. For α-glucosidase inhibition, the di-azomethine compound **12** (5-F, 2-OH substitution on one ring and 4-Br substitution on the other) demonstrated the most potent activity with an IC_{50} of 300 ± 22 μM. The mono-azomethine compound **8** (3,5-dimethoxy substitution) also showed strong inhibition (IC_{50} 343 ± 20 μM), both superior to the standard drug acarbose (IC_{50} 378.2 ± 0.12 μM). Molecular docking studies of the most active compound **12** revealed stable binding in the active site of α-glucosidase (PDB ID: 1XSK) involving conventional hydrogen bonding with Asp185 and Asp482, hydrophobic interactions, an RMSD of 1.8 Å, and a ΔG of −9.6 kcal mol^{-1}. Since Schiff bases are reported to exhibit both enzyme inhibition and antimicrobial properties, such multi-target activities may provide leads for the development of multifunctional therapeutic agents.

Received 27th January 2026
Accepted 25th February 2026

DOI: 10.1039/d6ra00719h

rsc.li/rsc-advances

Introduction

4-aminoantipyrine is an important organic compound that belongs to the class of pyrazole derivatives. Its derivatives have gained considerable interest due to their broad spectrum of biological activities, particularly in medicinal chemistry.[1–5] Several synthetic methods exist for 4-aminoantipyrine, including Claisen–Schmidt condensation from chalcones, reduction of azo compounds with hydrazine–hydrate, and reduction of 4-nitrosoantipyrine. The structural unit of 4-aminoantipyrine is an important constituent of many organic compounds and plays a significant role in analytical, coordination, and agriculture chemistry.[6,7] Schiff base metal complexes are especially important in drug discovery, as drugs administered as metal chelates often show enhanced activity compared to their free form.[8,9] Schiff bases of pyrazole are of great interest due to their wide range of biological activities,[10] especially 4-aminoantipyrine derivatives, which possess

[a]*Department of Chemistry, COMSATS University Islamabad, Abbottabad Campus, 22060, KPK, Pakistan. E-mail: majidbukhari@cuiatd.edu.pk*

[b]*Department of Chemistry, Government Postgraduate College No. 1, Abbottabad, KPK, Pakistan*

[c]*Department of Medical Microbiology, Faculty of Medicine, University of Tabuk, Tabuk 71491, Saudi Arabia*

[d]*Molecular Microbiology and Infectious Diseases Research Center, Faculty of Medicine, University of Tabuk, Tabuk 71491, Saudi Arabia*

[e]*Department of Biochemistry, Chandka Medical College (CMC), Shaheed Mohtarma Benazir Bhutto (SMBB) Medical University, Larkana, Sindh, Pakistan*

[f]*Department of Pharmaceutical Chemistry, College of Pharmacy, King Khalid University, Abha 62529, Saudi Arabia*

[g]*Natural and Medical Sciences Research Center, University of Nizwa, Birkat-ul-Mouz 616, Nizwa, Oman. E-mail: ajmalkhan@unizwa.edu.om; aharrasi@unizwa.edu.om; Tel: +968 25446328; +968-98957352*

[h]*Department of Chemical and Biological Engineering, College of Engineering, Korea University, Seongbuk-gu, 02841, Republic of Korea*

antipyretic action. Historically, these derivatives were first reported by Knorr in 1884, which led to their recognition as antipyrines.[11–17]

The derivatives of 4-aminoantipyrine have been applied in various medical fields, such as the treatment of oxidative stress and liver disease diagnosis. They also exhibit a wide range of pharmacological activities including antibacterial, antifungal, anticancer, anti-HIV, anti-inflammatory, anti-convulsant, and antiviral. The antibacterial potential of 4-aminoantipyrine derivatives has been reported to be active against Gram-positive and Gram-negative bacterial strains, for instance, *L. monocytogenes*, *S. tythi*, *K. pneumonia*,[18] *S. aureus*, *E. faecalis* and *E. coli*.[19] Literature further suggests that the nature and position of substituents significantly influence the antibacterial activity of antipyrine derivatives. In particular, Schiff base derivatives of 4-aminoantipyrine have shown remarkable antibacterial properties, often outperforming their parent compounds. The imine (C═N) linkage not only enhances lipophilicity but also facilitates better penetration through microbial cell membranes, thereby improving antibacterial efficacy.[20]

One of the most desired mechanisms in treating diabetes is postprandial hyperglycemia. α-Glucosidase inhibitors are key antidiabetic agents that delay carbohydrate digestion and regulate glucose absorption.[21,22] Schiff bases of 4-aminoantipyrine are noteworthy in coordination chemistry due to their versatile binding with aldehydes, ketones, and metal ions, which significantly contribute to their pharmacological behavior.[23] Recent studies highlight that Schiff base derivatives of 4-aminoantipyrine can act as potent α-glucosidase inhibitors. Their structural flexibility, combined with the ability to form stable chelates, allows them to bind effectively at the enzyme's active site, resulting in strong inhibitory action. This makes them promising candidates for developing novel antidiabetic agents.[24] We have previously reported the α-glucosidase inhibition potential of transition metal complexes of Schiff base derivatives of 4-aminoantipyrine, showing non-competitive inhibition.[25] This inhibition potential is attributed to the strong binding of these molecules within the enzyme's pocket, facilitated by the diverse functionalities present in their structures. The derivatives of aminoantipyrine, including metal complexes, are known to possess much better antidiabetic potential as compared to known antidiabetic candidates. These molecules tend to regulate α-glucosidase in the body.[26] The aim of the present study is to design and synthesize Schiff base derivatives of 4-aminoantipyrine, evaluate their antibacterial potential, and investigate their inhibitory activity against α-glucosidase. This dual approach is intended to explore multifunctional therapeutic candidates with both antimicrobial and antidiabetic applications.

Materials and methods

In this study, analytical grade chemicals along with pure solvents were used. All of the required chemicals and solvents were purchased from Sigma-Aldrich. In order to monitor the progress of reactions, thin layer chromatographic (TLC) plates (MERCK silica gel 60 F254) were used. The melting points of the obtained compounds were checked with the help of digital melting point apparatus; model SMP 10, OE/Digital (08-09)169/1 DMPA 09-01 and are expressed in (°C). The absorbance of all the compounds was measured in the UV-vis region in chloroform ($CHCl_3$) using 10 mm quartz in an instrument namely PG instrument T80 + UV-vis spectrophotometer. Fourier Transform-Infrared spectral analysis of all the compounds was performed with the help of Thermo-Nicolet 6700 P FT-IR spectrophotometer model 270 in ATR diamond window. On an advanced Bruker AM-400 MHz NMR spectrometer, the ^{1}H-NMR (ppm) spectra of the Schiff bases were recorded in $CDCl_3$. Chemical shift values (δ) were obtained in ppm and the coupling constant (J) was calculated in Hz. EcoBio Nutrient Broth and NEOGEN culture Media broth were used for bacterial growth. The source of *S. aureus* was a wound swab, and that of *S. typhi* was a typhoid fever. For the *in-vitro* enzyme inhibition assay, α-glucosidase enzyme derived from *E. coli* purchased from Creative Enzymes Cat. No. NATE-1177 was used.

Procedure for the synthesis of 4-aminoantipyrine based mono-azomethine schiff bases

The 4-aminoantipyrine-based mono-azomethine derivatives were synthesized by taking 100 mg of 4-aminoantipyrine in a beaker and dissolving it in a sufficient quantity of ethanol to obtain a clear solution. This solution was then transferred to a 250 mL round-bottom flask followed by the addition of equimolar quantities of the respective substituted aromatic aldehydes, the solutions of which had been prepared separately in beakers taking ethanol as solvent. A reflux condenser was attached to the reaction flask and the reaction mixture was refluxed each time for 6 hours. Reaction monitoring was performed each time by using normal-phase silica TLC plates developed in a solvent system of ethyl acetate and *n*-hexane (3 : 2) solvent system. The reaction completion was determined when a single spot of the product was obtained on the TLC plate. The products were obtained in a powdered form. Most of the products were yellow in color, while one product was off-white. The products were thoroughly washed with ethanol, dried, weighed, and their melting points were determined. Once the desired products were formed, the scale-up reactions of all compounds **(1–10)** were carried out.

Procedure for the synthesis of 4-aminoantipyrine based di-azomethine schiff bases

The 4-aminoantipyrine-based di-azomethine derivatives were synthesized in two steps. The first step was the same as described above, in which mono-azomethine derivatives of 4-aminoantipyrine were obtained. Mono-azomethine Schiff base molecules of 4-aminoantipyrine (**5**, **6** and **9**) were further used for the synthesis of di-azomethine compounds (**11–20**). The required compounds were synthesized by taking 100 mg of compounds (**5**, **6** and **9**) separately in beakers and dissolving them in 20 mL of ethanol to obtain clear solutions. Different substituted anilines were taken in equimolar amounts in different beakers and dissolved in ethanol to make clear solutions. Each aniline solution was added to the 250 mL round-

bottom flask along with a mono-azomethine solution. A reflux condenser was attached to each reaction flask and the reaction mixture was refluxed for 48 hours. After refluxing, the solvent was reduced to one-third of its volume and cooled to 0 °C. The obtained colored products were filtered, washed with ethanol, and dried. The melting points of the products were determined. Purification was done by column chromatography where required and scale-up reactions were conducted to increase the quantity of the obtained products.

Characterization

Compound 1: 4-(4-nitrobenzylideneamino)-2-methyl-1-phenyl-1,2-dihydropyrazol-5-one

Solid (dark yellow powder); yield = 82%; $R_f = 0.6$; (ethyl acetate: *n*-hexane, 3 : 2); m.p; = 254–256 °C; UV-vis (DMF) λ_{max} (410 nm); FT-IR (neat, cm^{-1}); ν = 1570 cm^{-1} (stretching wavenumber of imine group), 1637 cm^{-1} (stretching wavenumber of carbonyl group), 1414 cm^{-1} (stretching wavenumber of nitrogen–methyl bond); ^{1}H NMR (400 MHz, $CDCl_3$) δ (ppm); 8.27 (d, J = 8 Hz, 2H), 7.99 (d, J = 8 Hz, 2H), 9.82 (s, 1H), 2.54 (s, 1H), 3.25 (s, 1H), 7.40 (d, J = 8.0 Hz, 2H), 7.52 (t, J = 8 Hz, 2H), 7.37 (t, J = 8.0 Hz, 1H). ^{13}C NMR (100 MHz, $CDCl_3$) δ (ppm) 162.7, 155.4, 148.3, 142.0, 138.9, 136.2, 133.1, 129.2, 128.5, 126.8, 124.6, 124.3, 40.0.

Compound 2: 4-(3-nitrobenzylideneamino)-2-methyl-1-phenyl-1,2-dihydropyrazol-5-one

Solid (dark yellow powder); yield = 83%; $R_f = 0.7$; (ethyl acetate: *n*-hexane, 3 : 2); m.p; = 218–220 °C; UV-vis (DMF) λ_{max} (410 nm); FT-IR (neat, cm^{-1}); ν = 1571 cm^{-1} (stretching wavenumber of imine group), 1649 cm^{-1} (stretching wavenumber of carbonyl group), 1522 cm^{-1} and 1349 cm^{-1} (stretching wave number of nitro group), 1492 cm^{-1} (stretching wavenumber of nitrogen–methyl bond); ^{1}H NMR (400 MHz, $CDCl_3$) δ (ppm); 7.37 (t, J = 8 Hz, 1H), 7.51 (t, J = 8 Hz, 2H), 7.40 (d, J = 8 Hz, 2H), 2.55 (s, 3H), 3.25 (s, 3H), 9.8 (s, 1H), 8.07 (d, J = 8 Hz, 1H), 8.78 (d, J = 8.0 Hz, 1H), 7.58 (t, J = 8 Hz, 1H), 8.22 (d, J = 8.0H, 1H). ^{13}C NMR (100 MHz, $CDCl_3$) δ (ppm) 162.8, 153.7, 146.7, 138.9, 138.4, 136.2, 133.4, 130.6, 129.2, 129.0, 126.0, 124.6, 122.5, 122.1, 40.0.

Compound 3: 4-(4-hydroxybenzylideneamino)-2-methyl-1-phenyl-1,2-dihydropyrazol-5-one

Solid (yellowish powder); yield = 85%; $R_f = 0.6$; (ethyl acetate: *n*-hexane, 3 : 2); m.p; = 228–230 °C; UV-vis (DMF) λ_{max} (380 nm); FT-IR (neat, cm^{-1}); ν = 1578 cm^{-1} (stretching wave number of imine group), 1630 cm^{-1} (stretching wave number of carbonyl group), 1388 cm^{-1} (stretching wave number of carbon–nitrogen bond), 1459 cm^{-1} (stretching wave number of nitrogen–methyl bond); ^{1}H NMR (400 MHz, $CDCl_3$) δ (ppm); 7.34 (t, J = 8 Hz, 1H), 7.49 (t, J = 8 Hz, 2H), 7.43 (d, J = 8 Hz, 2H), 3.15 (s, 3H), 2.49 (s, 3H), 9.63 (s, 1H), 7.74 (d, J = 8 Hz, 2H), 6.86 (d, J = 8.0 Hz, 2H). ^{13}C NMR (100 MHz, $CDCl_3$) δ (ppm) 162.7, 157.4, 155.7, 138.9, 136.2, 133.1, 130.8, 129.7, 129.1, 126.3, 124.6, 116.1, 40.0.

Compound 4: 4-(4-methoxybenzylideneamino)-2-methyl-1-phenyl-1,2-dihydropyrazol-5-one

Solid (off white powder); yield = 86%; $R_f = 0.7$; (ethyl acetate: *n*-hexane, 3 : 2); m.p; = 245–249 °C; UV-vis (DMF) λ_{max} (390 nm); FT-IR (neat, cm^{-1}); ν = 1593 cm^{-1} (stretching wavenumber of imine group), 1640 cm^{-1} (stretching wavenumber of carbonyl group), 1377 cm^{-1} (stretching wavenumber of carbon–nitrogen bond), 2838 cm^{-1} (stretching wavenumber of methoxy group); ^{1}H NMR (400 MHz, $CDCl_3$) δ (ppm); 7.32 (t, J = 8 Hz, 1H), 7.49 (t, J = 8 Hz, 2H), 7.43 (d, J = 8 Hz, 2H), 3.14 (s, 3H), 2.49 (s, 3H), 9.73 (s, 1H), 7.83 (d, J = 8 Hz, 2H), 6.95 (d, J = 8.0 Hz, 2H), 3.87 (s, 3H). ^{13}C NMR (100 MHz, $CDCl_3$) δ (ppm) 162.8, 159.7, 155.6, 138.9, 136.2, 133.1, 132.3, 129.2, 126.4, 124.6, 114.8, 55.4, 40.0.

Compound 5: 4-(5-fluoro-2-hydroxybenzylideneamino)-2-methyl-1-phenyl-1,2-dihydropyrazol-5-one

Solid (yellow powder); yield = 80%; $R_f = 0.7$; (ethyl acetate: *n*-hexane, 3 : 2); m.p; = 209–212 °C; UV-vis (DMF) λ_{max} (405 nm); FT-IR (neat, cm^{-1}); ν = 1579 cm^{-1} (stretching wavenumber of imine group), 1650 cm^{-1} (stretching wavenumber of carbonyl group), 1158 cm^{-1} (stretching wavenumber of carbon–fluorine bond), 1377 cm^{-1} (stretching wavenumber of carbon–nitrogen bond), 1412 cm^{-1} (stretching wave number of nitrogen–methyl bond); ^{1}H NMR (400 MHz, $CDCl_3$) δ (ppm); 9.78 (s, 1H), 2.43 (s, 3H), 3.21 (s, 1H), 7.40 (d, J = 4 Hz, 2H), 7.51 (t, J = 4 Hz, 2H), 7.37 (t, J = 4 Hz, 1H), 6.99–7.06 (m, 2H), 6.89–6.92 (m, 1H). ^{13}C NMR (100 MHz, $CDCl_3$) δ (ppm) 162.9, 157.0, 156.3, 155.2, 153.2, 138.5, 136.2, 133.3, 129.2, 126.4, 124.6, 123.3, 119.6, 119.4, 118.3, 116.7, 116.6, 40.0.

Compound 6: 4-(2-hydroxy-5-methylbenzylideneamino)-2-methyl-1-phenyl-1,2-dihydropyrazol-5-one

Solid (yellowish powder); yield = 81%; $R_f = 0.7$; (ethyl acetate: *n*-hexane, 3 : 2); m.p; = 212–214 °C; UV-vis (DMF) λ_{max} (405 nm); FT-IR (neat, cm^{-1}); ν = 1576 cm^{-1} (stretching wave number of imine group), 1647 cm^{-1} (stretching wavenumber of carbonyl group), 1305 cm^{-1} (stretching wavenumber of carbon–nitrogen bond), 1426 cm^{-1} (stretching wavenumber of nitrogen–methyl bond); ^{1}H NMR (400 MHz, $CDCl_3$) δ (ppm); 7.36 (t, J = 8 Hz, 1H), 7.51 (t, J = 8 Hz, 2H), 7.42 (d, J = 8 Hz, 2H), 3.18 (s, 3H), 2.30 (s, 3H), 9.80 (s, 1H), 7.15 (s, 1H), 13.14 (s, 1H), 7.11 (d, J = 8 Hz, 1H), 6.87 (d, J = 8 Hz, 1H), 2.42 (s, 3H). ^{13}C NMR (100 MHz, $CDCl_3$) δ (ppm) 162.8, 157.2, 156.9, 138.5, 136.2, 133.3, 132.5, 132.1, 129.5, 129.2, 126.4, 124.6, 122.2, 116.8, 40.0, 20.6.

Compound 7: (*E*)-4-(4-phenylbenzylideneamino)-2,3-dimethyl-1-phenyl-1,2-dihydropyrazol-5-one

Solid (light golden powder); yield = 85%; $R_f = 0.8$; (ethyl acetate: *n*-hexane, 3 : 2); m.p; = 192–194 °C; UV-vis (DMF) λ_{max} (415 nm); FT-IR (neat, cm^{-1}); ν = 1571 cm^{-1} (stretching wavenumber of imine), 1640 cm^{-1} (stretching wavenumber of carbonyl group), 1377 cm^{-1} (stretching wavenumber of carbon–nitrogen bond), 1403 cm^{-1} (stretching wavenumber of nitrogen–methyl bond); ^{1}H NMR (400 MHz, $CDCl_3$) δ (ppm); 9.83 (s, 1H), 7.96 (d, J = 8 Hz, 2H), 7.68 (d, J = 8 Hz, 2H), 7.66 (t, J = 4 Hz, 2H), 7.33–7.40

(m, 4H), 7.43–7.53 (m, 4H). 3.18 (s, 3H), 2.53 (s, 3H), ^{13}C NMR (100 MHz, $CDCl_3$) δ (ppm) 162.8, 148.2, 146.0, 142.5, 140.3, 139.4, 135.6, 133.8, 129.0, 128.8, 128.4, 127.9, 127.8, 127.6, 126.5, 123.7, 36.3, 14.0.

Compound 8: (*E*)-4-(3,5-dimethoxybenzylideneamino)-2,3-dimethyl-1-phenyl-1,2-dihydropyrazol-5-one

Solid (light yellowish powder); yield = 83%; R_f = 0.8; (ethyl acetate: *n*-hexane, 3 : 2); m.p; = 166–168 °C; UV-vis (DMF) λ_{max} (395 nm); FT-IR (neat, cm^{-1}); ν = 1583 cm^{-1} (stretching wavenumber of imine group), 1635 cm^{-1} (stretching wavenumber of carbonyl group), 1370 cm^{-1} (stretching wavenumber of carbon–nitrogen bond), 1415 cm^{-1} (stretching wavenumber of nitrogen–methyl bond), 2839 cm^{-1} (stretching wavenumber of methoxy group); ^{1}H NMR (400 MHz, $CDCl_3$) δ (ppm); 9.70 (s, 1H), 3.86 (s, 1H), 6.53 (t, J = 4 Hz, 1H), 7.05 (d, J = 4 Hz, 2H), 7.42 (d, J = 8 Hz, 2H), 7.50 (t, J = 8 Hz, 2H), 7.34 (t, J = 8 Hz, 1H), 3.17 (s, 3H), 2.51 (s, 3H). ^{13}C NMR (100 MHz, $CDCl_3$) δ (ppm) 162.7, 161.7, 148.0, 145.7, 141.4, 135.7, 133.7, 129.1, 126.5, 123.7, 107.0, 102.19, 55.3, 36.3, 13.9.

Compound 9: 4-(2-hydroxybenzylideneamino)-1,5-dimethyl-2-phenyl-1,2-dihydropyrazol-3-one

Solid (yellow powder); yield = 80%; R_f = 0.59; (ethyl acetate: *n*-hexane, 3 : 2); m.p; = 198–200 °C; UV-vis (DCM) λ_{max} (380 nm); FT-IR (neat, cm^{-1}); ν = 1628 cm^{-1} (stretching wavenumber of imine group), 1486 cm^{-1} (stretching wavenumber of C=$C_{aromatic}$), 2924 cm^{-1} (stretching wavenumber of =C–H), 1358 cm^{-1} (stretching wavenumber of carbon–nitrogen bond), 3345 cm^{-1} (stretching wavenumber of hydroxyl group), 1089 cm^{-1} (stretching wavenumber of carbon–oxygen bond); ^{1}H NMR (400 MHz, $CDCl_3$) δ (ppm); 13.25 (s, 1H), 9.72 (s, 1H), 7.46 (t, J = 8.0 Hz, 2H), 7.43 (d, J = 8 Hz, 1H), 7.42 (d, J = 8.0 Hz, 2H), 7.40 (m, 1H), 6.65 (d, J = 8.0 Hz, 1H), 6.57 (s, 1H), 3.80 (s, 3H), 3.20 (s, 3H), 2.43 (s, 3H). ^{13}C NMR (100 MHz, $CDCl_3$) δ (ppm) 162.7, 160.0, 149.6, 145.7, 135.5, 133.6, 132.4, 130.1, 129.2, 126.6, 125.5, 124.2, 121.2, 117.5, 36.2, 14.0.

Compound 10: 4-((2-hydroxy-4-methoxybenzylidene)amino)-1,5-dimethyl-2-phenyl-1,2-dihydro-3*H*-pyrazol-3-one

Solid (yellow powder); yield = 80%; R_f = 0.6; (ethyl acetate: *n*-hexane, 3 : 2); m.p. = 128–200 °C; UV-vis ($CDCl_3$) λ_{max} (380 nm) = 380; FT-IR (neat, cm^{-1}); ν = 1628 cm^{-1} (stretching wavenumber of imine group), 1486 cm^{-1} (stretching wavenumber of C=$C_{aromatic}$), 2924 cm^{-1} stretching wavenumber of =C–H), 1358 cm^{-1} (stretching wavenumber of carbon–nitrogen bond), 3345 cm^{-1} (stretching wavenumber of hydroxyl group), 1089 cm^{-1} (stretching wavenumber of carbon–oxygen bond); ^{1}H NMR (400 MHz, $CDCl_3$) δ (ppm) = 13.25 (s, 1H), 9.72 (s, 1H), 7.46 (t, J = 8.0 Hz, 2H), 7.43 (d, J = 8 Hz, 1H), 7.42 (d, J = 8.0 Hz, 2H), 7.40 (m, 1H), 6.65 (d, J = 8.0 Hz, 1H), 6.57 (s, 1H), 3.80 (s, 3H), 3.20 (s, 3H), 2.43 (s, 3H). ^{13}C NMR (100 MHz, $CDCl_3$) δ (ppm) 163.1, 162.9, 158.9, 149.6, 145.7, 135.8, 133.7, 130.4, 129.1, 126.2, 123.9, 119.9, 106.7, 101.8, 55.5, 36.2, 13.9.

Compound 11: (*Z*)-2-((1,5-dimethyl-2-phenyl-3-(phenylimino)-2,3-dihydro-1*H*-pyrazol-4-ylimino)methyl)-4-fluorophenol

Solid (orange powder); yield = 60%; R_f = 0.6; (ethyl acetate: *n*-hexane, 3 : 2); m.p; = 113–115 °C; UV-vis ($CDCl_3$) λ_{max} (391 nm); FT-IR (neat, cm^{-1}); ν = 1629 cm^{-1} (stretching wavenumber of imine group), 1484 cm^{-1} (stretching waven μMber of C=$C_{aromatic}$), 3054 cm^{-1} (stretching wavenumber of =C–H), 1354 cm^{-1} (stretching wavenumber of carbon–nitrogen bond), 1134 cm^{-1} (stretching wavenumber of carbon–fluorine bond), 3248 cm^{-1} (stretching wavenumber of hydroxyl group); ^{1}H NMR (400 MHz, $CDCl_3$) δ (ppm); 11.12 (s, 1H), 10.81 (s, 1H), 7.48 (d, J = 4.0 Hz, 1H), 7.45 (dd, J = 8.0 Hz, 2H), 7.35 (t, J = 8.0 Hz, 1H), 7.31 (d, J = 8.0 Hz, 2H), 7.16 (m, 1H), 7.15 (d, J = 8.0 Hz, 1H), 7.13 (dd, J = 8.0, 4.0 Hz, 2H), 7.01 (d, J = 8.0 Hz, 2H), 6.99 (t, J = 8.0 Hz, 1H), 1.28 (s, 1H), 1.00 (s, 3H). ^{13}C NMR (100 MHz, $CDCl_3$) δ (ppm) 156.4, 156.1, 156.1, 155.3, 154.4, 150.5, 150.5, 146.0, 141.1, 138.9, 128.9, 128.8, 127.7, 126.1, 124.4, 124.2, 124.1, 123.8, 121.0, 119.9, 119.7, 118.2, 118.1, 117.4, 117.3, 36.3, 14.1.

Compound 12: (*Z*)-2-((3-(4-bromophenylimino)-1,5-dimethyl-2-phenyl-2,3-dihydro-1*H*-pyrazol-4-ylimino)methyl)-4-fluorophenol

Solid (orange powder); yield = 75%; R_f = 0.59 (ethyl acetate: *n*-hexane, 3 : 2); m.p; = 133–135 °C; UV-vis ($CDCl_3$) λ_{max} (391 nm); FT-IR; ν = 1615 cm^{-1} (stretching wavenumber of imine group), 1482 cm^{-1} (stretching wavenumber of C=$C_{aromatic}$), 3075 cm^{-1} (stretching wavenumber of =C–H), 1348 cm^{-1} (stretching wavenumber of carbon–nitrogen bond), 1142 cm^{-1} (stretching wavenumber of carbon–fluorine bond), 3057 cm^{-1} (stretching wavenumber of hydroxyl group); ^{1}H NMR (400 MHz, $CDCl_3$) δ (ppm) = 12.79 (s, 1H), 9.87 (s, 1H), 7.58 (dd, J = 8.0, 4.0 Hz, 2H), 7.18 (d, J = 8.0 Hz, 2H), 7.16 (t, J = 8.0 Hz, 1H), 7.15 (d, J = 4.0 Hz, 1H), 7.13 (m, 1H), 7.10 (d, J = 8.0 Hz, 1H), 7.02 (d, J = 8.0 Hz, 2H), 6.99 (d, J = 8.0 Hz, 2H), 3.50 (s, 3H), 3.20 (s, 1H). ^{13}C NMR (100 MHz, $CDCl_3$) δ (ppm) 156.2, 155.6, 155.6, 154.2, 153.8, 151.0, 151.0, 145.3, 140.7, 138.7, 131.8, 129.0, 127.5, 126.2, 124.1, 124.0, 123.6, 122.5, 122.4, 120.0, 119.8, 118.0, 117.9, 117.4, 117.2, 36.3, 14.1.

Compound 13: (*Z*)-2-((3-(4-chlorophenylimino)-1,5-dimethyl-2-phenyl-2,3-dihydro-1*H*-pyrazol-4-ylimino) methyl)-4-fluorophenol

Solid (orange powder); yield = 70%; R_f = 0.6 (ethyl acetate: *n*-hexane, 3 : 2); = 128–130 °C; UV-vis ($CDCl_3$) λ_{max} (384 nm); FT-IR (neat, cm^{-1}); ν = 1615 cm^{-1} (stretching wavenumber of imine), 1481 cm^{-1} (stretching wavenumber of C=$C_{aromatic}$), 3055 cm^{-1} (stretching wavenumber of =C–H), 1354 cm^{-1} (stretching wavenumber of carbon–nitrogen bond), 1145 cm^{-1} (stretching wavenumber of carbon–fluorine bond), 3389 cm^{-1} (stretching wavenumber of hydroxyl group); ^{1}H NMR (400 MHz, $CDCl_3$) δ (ppm) = 12.78 (s, 1H), 9.88 (s, 1H), 7.42 (dd, J = 8.0, 4.0 Hz, 2H), 7.25 (d, J = 8.0 Hz, 2H), 7.16 (t, J = 8.0 Hz, 1H), 7.15 (d, J = 4.0 Hz, 1H), 7.14 (m, 1H), 7.11 (d, J = 8.0 Hz, 1H), 7.02 (2H, d, J = 8.0 Hz, 2H), 6.99 (d, J = 8.0 Hz, 2H), 3.24 (s, 3H), 1.28 (s, 3H). ^{13}C NMR (100 MHz, $CDCl_3$) δ (ppm) 156.4, 155.5, 155.4, 154.4, 153.8,

151.0, 151.0, 144.6, 141.1, 138.7, 131.7, 129.0, 127.7, 126.2, 124.1, 124.0, 123.8, 122.0, 119.9, 119.7, 118.1, 118.0, 117.4, 117.2, 36.4, 14.0.

Compound 14: (*Z*)-4-fluoro-2-((3-(4-iodophenylimino)-1,5-dimethyl-2-phenyl-2,3-dihydro-1*H*-pyrazol-4-ylimino) methyl) phenol

Solid (orange powder); yield = 80%; R_f = 0.6 (ethyl acetate: *n*-hexane, 3 : 2); m.p; = 118–200 °C; UV-vis ($CDCl_3$) λ_{max} (384 nm); FT-IR (neat, cm^{-1}); ν = 1613 cm^{-1} (stretching wavenumber of imine group), 1482 cm^{-1} (stretching wavenumber of C=$C_{aromatic}$), 3059 cm^{-1} (stretching wavenumber of =C–H), 1350 cm^{-1} (stretching wavenumber of carbon–nitrogen bond), 1142 cm^{-1} (stretching wavenumber of carbon-fluorine), 3342 cm^{-1} (stretching wavenumber of hydroxyl group); ^{1}H NMR (400 MHz, $CDCl_3$) δ (ppm) = 12.78 (s, 1H), 9.78 (s, 1H), 7.65 (dd, J = 8.0, 4.0 Hz, 2H), 7.62 (d, J = 8.0 Hz, 2H), 7.48 (m, 1H), 7.47 (d, J = 8.0 Hz, 2H), 7.45 (d, J = 8.0 Hz, 2H), 7.15 (d, J = 4.0 Hz, 1H), 6.80 (m, 1H), 6.45 (d, J = 8.0 Hz, 1H), 3.50 (s, 3H), 2.45 (s, 3H). ^{13}C NMR (100 MHz, $CDCl_3$ δ (ppm) 157.0, 155.5, 154.9, 147.6, 147.0, 146.9, 146.2, 139.0, 138.8, 137.9, 128.9, 127.5, 126.2, 124.3, 124.3, 123.0, 120.0, 119.8, 117.8, 116.8, 116.6, 94.3, 36.3, 13.5.

Compound 15: 2-((((*Z*)-1,5-dimethyl-2-phenyl-3-(phenylimino)-2,3-dihydro-1*H*-pyrazol-4-yl)imino)methyl)-4-methylphenol

Solid (orange to yellow powder); yield = 55%; R_f = 0.5; (ethyl acetate: *n*-hexane, 3 : 2); m.p; = 100–102 °C; UV-vis ($CDCl_3$) λ_{max} (385 nm); FT-IR (neat, cm^{-1}); ν = 1617 cm^{-1} (stretching wavenumber of imine group), 1485 cm^{-1} (stretching wavenumber of C=$C_{aromatic}$), 2918 cm^{-1} (stretching wavenumber of carbon–hydrogen bond), 1354 cm^{-1} (stretching wavenumber of carbon–nitrogen bond), 3058 cm^{-1} (stretching wavenumber of hydroxyl group), 1070 cm^{-1} (stretching wavenumber of carbon–oxygen bond); ^{1}H NMR (400 MHz, $CDCl_3$) δ (ppm) = 12.78 (s, 1H), 9.88 (s, 1H), 7.47 (s, 1H), 7.45 (dd, J = 8.0, 4.0 Hz, 2H), 7.33 (m, 1H), 7.30 (d, J = 8.0 Hz, 2H), 7.23 (dd, J = 8.0, 4.0 Hz, 2H), 7.21 (d, J = 8.0 Hz, 2H), 6.99 (d, J = 8.0 Hz, 1H), 6.97 (d, J = 8.0 Hz, 1H), 6.91 (m, 1H), 3.25 (s, 3H), 2.35 (s, 6H). ^{13}C NMR (100 MHz, $CDCl_3$) δ (ppm) 157.5, 155.3, 149.7, 146.0, 141.1, 138.9, 132.7, 131.8, 129.6, 128.9, 128.8, 127.7, 126.1, 124.4, 123.8, 123.4, 121.0, 116.6, 36.3, 20.6, 14.1.

Compound 16: 2-((((*Z*)-3-((4-bromophenyl) imino)-1,5-dimethyl-2-phenyl-2,3-dihydro-1*H*-pyrazol-4-yl)imino)methyl)-4-methylphenol

Solid (orange powder); yield = 70%; R_f = 0.6; (ethyl acetate: *n*-hexane, 3 : 2); m.p; = 172–174 °C; UV-vis ($CDCl_3$) λ_{max} (388 nm); FT-IR (neat, cm^{-1}); ν = 1613 cm^{-1} (stretching wavenumber of imine group), 1481 cm^{-1} (stretching wavenumber of C=$C_{aromatic}$), 3075 cm^{-1} (stretching wavenumber of =C–H), 1351 cm^{-1} (stretching wavenumber of carbon–nitrogen bond), 3521 cm^{-1} (stretching wavenumber of hydroxyl group), 1067 cm^{-1} (stretching wavenumber of carbon–oxygen bond); ^{1}H NMR (400 MHz, $CDCl_3$) δ (ppm) = 12.75 (s, 1H), 9.87 (s, 1H), 7.56 (dd, J = 8.0, 4.0 Hz, 2H), 7.35 (m, 1H), 7.24 (s, 1H), 7.21 (d, J = 8.0 Hz, 2H), 7.18 (d, J = 8.0 Hz, 2H), 6.97 (d, J = 8.0 Hz, 2H), 6.93 (d, J = 8.0 Hz, 1H), 6.91 (d, J = 8.0 Hz, 1H), 3.00 (s, 3H), 2.35 (s, 6H). ^{13}C NMR (100 MHz, $CDCl_3$) δ (ppm) 157.1, 153.8, 149.7, 145.3, 140.7, 138.7, 133.3, 132.0, 131.8, 129.5, 129.0, 127.5, 126.2, 123.6, 123.4, 122.5, 122.4, 116.6, 36.3, 20.6, 14.1.

Compound 17: 2-((((*Z*)-3-((4-chlorophenyl) imino)-1,5-dimethyl-2-phenyl-2,3-dihydro-1*H*-pyrazol-4-yl)imino)methyl)-4-methylphenol

Solid (yellow powder); yield = 55%; R_f = 0.5; (ethyl acetate: *n*-hexane, 3 : 2); m.p; = 102–104 °C; UV-vis ($CDCl_3$) λ_{max} (385 nm); FT-IR (neat, cm^{-1}); ν = 1645 cm^{-1} (stretching wavenumber of imine group), 1481 cm^{-1} (stretching wavenumber of C=$C_{aromatic}$), 3068 cm^{-1} (stretching wavenumber of =C–H), 1367 cm^{-1} (stretching wavenumber of carbon–nitrogen bond), 3368 cm^{-1} (stretching wavenumber of hydroxyl group), 1060 cm^{-1} (stretching wavenumber of carbon–oxygen bond); ^{1}H NMR (400 MHz, $CDCl_3$) δ (ppm) = 12.82 (s, 1H), 9.87 (s, 1H), 7.41 (d, J = 8.0 Hz, 2H), 7.35 (t, J = 8.0 Hz, 1H), 7.23 (dd, J = 8.0, 4.0 Hz, 1H), 7.21 (d, J = 8.0 Hz, 1H), 6.96 (d, J = 8.0 Hz, 2H), 6.93 (d, J = 8.0 Hz, 1H), 6.91 (d, J = 8.0 Hz, 1H), 3.22 (s, 3H), 2.35 (s, 6H). ^{13}C NMR (100 MHz, $CDCl_3$ δ (ppm) 157.4, 153.8, 149.7, 144.6, 141.1, 138.7, 132.6, 132.0, 131.7, 129.6, 129.0, 127.7, 126.2, 123.8, 123.4, 122.0, 116.5, 36.4, 20.6, 14.0.

Compound 18: 2-((((*Z*)-1,5-dimethyl-3-((4-nitrophenyl)imino)-2-phenyl-2,3-dihydro-1*H*-pyrazol-4-yl)imino)methyl)-4-methylphenol

Solid (yellow powder); yield = 70%; R_f = 0.6; (ethyl acetate: *n*-hexane, 3 : 2); m.p; = 114–116 °C; UV-vis ($CDCl_3$) λ_{max} (386 nm); FT-IR (neat, cm^{-1}); ν = 1612 cm^{-1} (stretching wavenumber of imine group), 1485 cm^{-1} (stretching wavenumber of C=$C_{aromatic}$), 3059 cm^{-1} (stretching wavenumber of =C–H), 1358 cm^{-1} (stretching wavenumber of carbon–nitrogen bond), 3358 cm^{-1} (stretching wavenumber of hydroxyl group), 1070 cm^{-1} (stretching wavenumber of carbon–oxygen bond); ^{1}H NMR (400 MHz, $CDCl_3$) δ (ppm) = 9.88 (s, 1H), 8.68 (s, 1H), 7.74 (d, J = 8.0 Hz, 2H), 7.72 (dd, J = 8.0, 4.0 Hz, 2H), 7.58 (m, 1H), 7.56 (d, J = 8.0 Hz, 2H), 7.54 (d, J = 8.0 Hz, 2H), 7.22 (d, J = 8.0 Hz, 1H), 7.16 (d, J = 8.0 Hz, 1H), 6.96 (s, 1H), 2.34 (s, 3H), 1.00 (s, 6H). ^{13}C NMR (100 MHz, $CDCl_3$) δ (ppm) 157.2, 154.0, 150.3, 149.8, 147.0, 141.1, 138.9, 132.6, 132.2, 129.6, 129.1, 127.7, 126.4, 124.5, 123.8, 123.4, 121.6, 116.6, 36.4, 20.6, 14.0.

Compound 19: (*Z*)-2-((1,5-dimethyl-2-phenyl-3-(phenylimino)-2,3-dihydro-1*H*-pyrazol-4-ylimino)methyl)-5-methoxyphenol

Solid (yellowish powder); yield = 70%; R_f = 0.6; (ethyl acetate: *n*-hexane, 3 : 2); m.p = 102–104 °C; UV-vis ($CDCl_3$) λ_{max} (386 nm); FT-IR (neat, cm^{-1}); ν = 1611 cm^{-1} (stretching waven μMber of imine group), 1482 cm^{-1} (stretching wavenumber of C=$C_{aromatic}$), 3059 cm^{-1} (stretching wavenumber of =C–H), 1351 cm^{-1} (stretching wavenumber of carbon–nitrogen bond), 3208 cm^{-1} (stretching wavenumber of hydroxyl group), 1080 cm^{-1} (stretching wavenumber of carbon–oxygen bond); ^{1}H NMR (400 MHz, $CDCl_3$) δ (ppm) = 13.64 (s, 1H), 11.41 (s, 1H),

7.47 (d, J = 8.0 Hz, 1H), 7.45 (dd, J = 8.0, 4.0 Hz, 2H),7.34 d, J = 8.0 Hz, 2H), 7.32 (t, J = 8.0 Hz, 1H), 7.32 (t, J = 8.0 Hz, 1H), 7.27 (m, 2H), 7.21 (d, J = 8.0 Hz, 2H), 6.45 (s, 1H), 6.43 (d, J = 8.0 Hz, 1H), 3.59 (s, 3H), 2.24 (s, 3H), 1.25 (s, 3H). ^{13}C NMR (100 MHz, $CDCl_3$) δ (ppm) 163.0, 158.7, 155.3, 150.2, 146.2, 141.1, 138.7, 130.1, 129.0, 128.8, 127.7, 126.1, 124.4, 123.8, 121.0, 117.7, 107.0, 102.2, 55.5, 36.4, 14.1.

Compound 20: 2-((((*Z*)-3-((4-chlorophenyl)imino)-1,5-dimethyl-2-phenyl-2,3-dihydro-1*H*-pyrazol-4-yl)imino) methyl)-5-methoxyphenol

Solid (yellow powder); yield = 55%; R_f = 0.6; (ethyl acetate: *n*-hexane, 3 : 2); m.p; = 126–128 °C; UV-vis ($CDCl_3$) λ_{max} (384 nm); FT-IR (neat, cm^{-1}); ν = 1619 cm^{-1} (stretching wavenumber of imine group), 1482 cm^{-1} (stretching wavenumber of C=C$_{aromatic}$), 3050 cm^{-1} (stretching wavenumber of =C–H), 1358 cm^{-1} (stretching wavenumber of carbon–nitrogen bond), 3345 cm^{-1} (stretching wavenumber of hydroxyl group), 1067 cm^{-1} (stretching wavenumber of carbon–oxygen bond); ^{1}H NMR (400 MHz, $CDCl_3$) δ (ppm) = 11.51 (s, 1H), 9.74 (s, 1H), 8.53 (d, J = 8.0 Hz, 1H), 7.43 (m, 1H), 7.40 (dd, J = 8.0, 4.0 Hz, 2H), 7.30 (d, J = 8.0 Hz, 2H), 7.21 (d, J = 8.0 Hz, 2H), 6.54 (d, J = 8.0 Hz, 2H), 6.51 (d, J = 8.0 Hz, 1H), 6.45 (s, 1H), 3.80 (s, 3H), 1.34 (s, 3H), 1.27 (s, 3H). ^{13}C NMR (100 MHz, $CDCl_3$) δ (ppm) 162.7, 158.7, 154.0, 150.8, 144.6, 141.1, 138.9, 132.1, 130.3, 129.1, 129.0, 127.7, 126.4, 123.8, 122.0, 117.7, 107.2, 102.1, 55.5, 36.4, 14.0.

Antibacterial potential

The synthesized compounds were investigated for possible antibacterial potential using the agar well diffusion method. The *in-vitro* biological screening effects of the synthesized compounds were tested against the bacteria *Salmonella typhi* and *Staphylococcus aureus*. The stock solution for each sample was obtained after sample dissolution in DMSO. The agar medium was prepared in distilled water and autoclaved at 121 °C for 25 min. On the agar medium wells were prepared and then filled with tested sample using a micropipette. The incubation of plates was carried out at 37 °C and the diameter of inhibition zones was measured. Ciprofloxacin was taken as a positive control (standard).

α-Glucosidase inhibition assay

For the enzyme inhibition assay, α-glucosidase enzyme derived from *E. coli* purchased from Creative Enzymes, Cat. No. NATE-1177, was used, and the assay was performed following a reported method with slight modifications. In a 96-well plate, 120 μL of sodium phosphate buffer (pH = 7) was added, and then 20 μL of enzyme (2 U mL^{-1}) was added. Then 20 μL of test compound (0.5 mM) was added followed by immediate incubation for a time of 15 min at 37 °C. In sequence, substrate *p*-nitrophenyl glucopyranoside (*p*NPG) (20 μL, 1 mM) was taken in each well, and dissolved in buffer. The reaction mixture was again subjected to incubation for about 15 min at 37 °C. The termination of the reaction was achieved by adding 20 μL of 0.1 mM sodium carbonate (Na_2CO_3), so that the final volume becomes 200 μL. The activity of the enzyme was measured spectrophotometrically at 405 nm by measuring the concentration of the product formed. Triplicate analysis was done for each sample under consideration. The % inhibition and IC_{50} results were calculated and compared with positive control (Acarbose).

Molecular docking studies

The crystal structure of the enzyme α-glucosidase (PDB ID:1XSK) was retrieved from the Protein Data Bank (PDB). Docking of synthesized molecules in the active site was carried out using MOE-Dock. The triangle matcher placement method was used with the London dG scoring function with default parameters. Refinement was carried out using the Induced-Fit method and rescoring by Affinity dG. The maximum number of retained poses was 10 during docking. Final poses were selected based on binding energies, (root means square deviations) RMSD values, and molecular interactions. To obtain 2D and 3D docking poses of complexes, MOE was used which automatically creates 2D poses with known 3D structures.

MD simulation studies

Molecular dynamics (MD) simulation is a computational tool used to numerically solve the equations of motion for atoms in a specified reference frame. In this study, the Desmond software was employed to simulate a protein-ligand complex over 100 nanoseconds using the TIP3P solvent model. To accurately represent molecular interactions, the OPLS3 force field was applied, along with periodic boundary conditions (PBC) to mimic an infinite system.[27] An orthorhombic solvation box containing TIP3P water molecules was constructed to solvate the system, and neutralization was achieved by adding NaCl counter ions at a concentration of 0.15 M. The system underwent a 2000-step energy minimization using the steepest descent method to resolve steric clashes. It was then equilibrated to 300 K and 1.01 bar under an isothermal–isobaric (NPT) ensemble. Short-range van der Waals interactions were considered within a 10 Å cutoff. Pressure and temperature stability were maintained using the Martyna–Tobias–Klein barostat and the Nosé–Hoover thermostat.[28] The production run of 100 ns was performed with trajectory snapshots saved every 100 picoseconds. The particle mesh Ewald method was utilized to calculate electrostatic interactions, with a 2-femtosecond time step ensuring precision.[29] Finally, the simulated trajectories of the protein-ligand complex were analyzed using the Desmond simulation diagram protocol.[30]

Results and discussion

Synthesis of 4-aminoantipyrine based mono-azomethine schiff bases

The 4-aminoantipyrine derivatives were synthesized by reacting 4-aminoantipyrine with various substituted benzaldehydes (**1**–**10**) in the presence of ethanol as shown in Scheme 1. Each time the reaction mixture was refluxed for 6 hours, and colored powdered compounds were filtered and washed with ethanol.

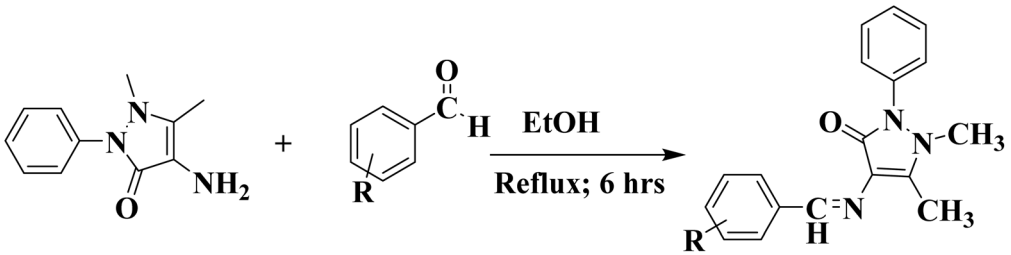

1. R = 4-NO_2 4. R = 4-OCH_3 7. R = 4-C_6H_6
2. R = 3-NO_2 5. R = 5-F, 2-OH 8. R = 3-OCH_3, 5-OCH_3
3. R = 4-OH 6. R = 2-OH, 5-CH_3 9. R = 2-OH
10. R = 2-OH, 4-OCH_3

Scheme 1 General synthetic scheme for the synthesis of mono-azomethine Schiff bases of 4-aminoantipyrine.

Synthesis of 4-aminoantipyrine based di-azomethine schiff bases

Mono-azomethine Schiff base molecules of 4-aminoantipyrine (**5**, **6** and **9**) were further used for the synthesis of di-azomethine compounds (**11–20**) as given in Scheme 2. The required compounds were synthesized by dissolving compounds (**5**, **6** and **9**) in 20 mL of ethanol and heating them under reflux for about 48 hours. After refluxing, the solvent was reduced to one-third of its volume and cooled to 0 °C. The obtained products were colored powders, it was filtered, and washed with ethanol.

The 4-aminoantipyrine-based mono-azomethine (**1–10**) and di-azomethine (**11–20**) Schiff bases were synthesized according to the generalized synthetic Schemes 1 and 2, respectively. All the compounds were colored and soluble in $CHCl_3$ and DMSO. The structural elucidation of all of the newly synthesized Schiff bases was carried out using UV-vis, FT-IR, ^{1}H NMR and ^{13}C NMR spectroscopic techniques.

The characteristic signals of the imine group stretching appeared at 1570 cm^{-1} in the case of compound **1** and up to 1649 cm^{-1} in the case of compound **17** (Fig. 1). These signals always appeared as sharp and distinct signals. In mono-azomethine series of compounds, in almost all cases, the characteristic signal showed the highest percent transmittance whereas in the di-azomethine series, the signals were still sharp but had lower percent transmittance than in the first series. This indicates that the introduction of a second azomethine group results in the appearance of other signals sharper in terms of percent transmittance compared to the imine functionality. The characteristic proton signal of the imine in the case of mono-azomethine was observed in the range of 9.63 ppm (compound **3**) to 9.83 ppm (compound **7**). All other compounds of the mono-azomethine series showed imine proton signals within the above ppm range. This signal always appeared as a singlet due to the non-availability of neighboring protons. Similarly, the incorporation of respective aldehydes into the final compounds was evident from the aromatic signals. For instance, the aromatic signals appearing at and above 8 ppm in the case of compound **1** and compound **2**

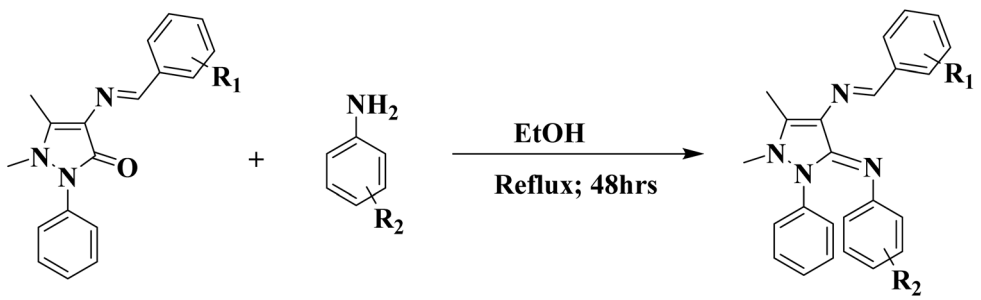

11. R_1 = 5-F, 2-OH; R_2 = H
12. R_1 = 5-F, 2-OH; R_2 = 4-Br
13. R_1 = 5-F, 2-OH; R_2 = 4-Cl
14. R_1 = 5-F, 2-OH; R_2 = 4-I
15. R_1 = 2-OH, 5-CH_3; R_2 = H
16. R_1 = 2-OH, 5-CH_3; R_2 = 4-Br
17. R_1 = 2-OH, 5-CH_3; R_2 = 4-Cl
18. R_1 = 2-OH, 5-CH_3; R_2 = 4-NO_2
19. R_1 = 2-OH, 4-OCH_3; R_2 = H
20. R_1 = 2-OH, 4-OCH_3; R_2 = 4-Cl

Scheme 2 General synthetic scheme for the synthesis of di-azomethine Schiff bases of 4-aminoantipyrine.

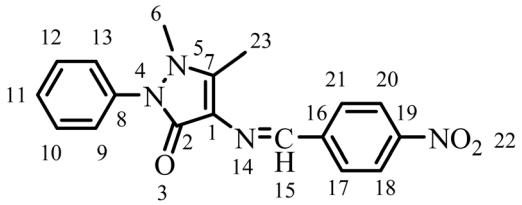

Fig. 1 Structure of compound **1** for the discussion of NMR signals.

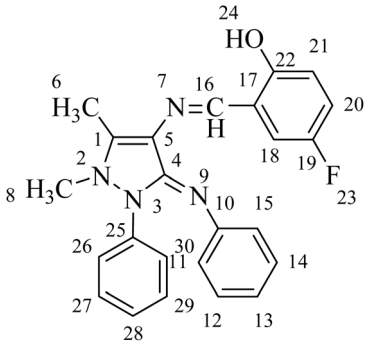

Fig. 2 Structure of compound **11** for the discussion of NMR signals.

belonged to the protons of nitroaromatic rings of the reactant aldehydes. The small signals appearing at 9.86 ppm in the case of compound **3** and at 13.14 in the case of compound **6** belonged to the hydroxyl groups of the respective attached aldehydes; a signal at 3.87 ppm corresponded to methoxy protons in compound **4** and fluorine coupling appeared in the NMR of compound **5** where fluorine was part of the aldehyde moiety. Similar characteristic signals are also noticeable in the other members of this series.

For reference, the NMR signals of compound **1** are discussed here in detail. In the ^{1}H-NMR spectrum of compound **1**, a singlet signal was observed at δ 9.82 ppm (downfield) attributed to the proton of imine group (position 15). Protons at position 18 and 20 appeared downfield due to the electron withdrawing effect of neighboring nitro group. These deshielded protons, being equivalent in the same electronic environment, produced a doublet at δ 8.27 ppm. Similarly, protons at positions 17 and 21, also equivalent gave doublet signals at around δ 7.99 ppm. Protons at positions 13 and 09, each having one neighboring proton, exhibited doublets at δ 7.40 ppm. The signals are in agreement with literature.[7] Two triplets were observed for protons at positions 10, 11 and 12. Protons at positions 10 and 12 being equivalent, appeared as a triplet at δ 7.20 ppm, while the proton at position 11, present in their vicinity, gave a triplet at δ 7.37 ppm. Two singlets corresponding to six protons of the two methyl groups were also noted. These two methyl groups, being in slightly different electronic environments, appeared at different shifts. The proton at position 6 was slightly deshielded and appeared downfield relative to the proton at position 23 due to its attachment with the nitrogen *i.e.* electronegative atom. The above-described signals are in good agreement with literature values.[31]

In the case of the compounds of di-azomethine series, the characteristic proton signals of imine groups appear in the range of 9.78–10.81 ppm. In some cases, these protons appeared in relatively shielded regions, as seen for compounds **17** and **19**. The hydroxyl groups in these compounds showed further downfield resonances, appearing as relatively short and broad signals. The influence of substituents was also evident, halogens at the R_2 position (compound **12** to **14** and **16**, **17**) and the nitro group in case of compound 18 produced characteristic deshielding effects on the neighboring protons. In particular, the aromatic protons in compound 18 were significantly deshielded due to the strong electron-withdrawing nature of the nitro functionality for reference, the NMR signals of compound **11** are discussed in detail (Fig. 2). The ^{1}H-NMR spectrum of compound **11** revealed that the proton (imine group) at position 16 appears as a singlet with the chemical shift value at δ 10.81 ppm (downfield). This signal is in agreement with the literature.[32] The proton at position 18 appeared as a doublet at chemical shift of δ 7.48 ppm. Protons at position 26 and 30 have one neighboring proton each, therefore, they showed doublets at δ 7.31 ppm. Protons at position 27 and 29 are in similar environment and exhibited a doublet of doublets at δ 7.45 ppm. Two triplets were observed for protons at position 13 and 28. Proton at position 28 gave a triplet at δ 7.35 ppm, while proton at position 13 appeared as a triplet at δ 6.99 ppm. Protons at position 11 and 15 are equivalent and produced a doublet at δ 7.01 ppm. Similarly, protons at 12 and 14 are also equivalent and showed a doublet of doublets at δ 7.13 ppm. The proton at position 20 appeared as a multiplet at δ 7.16 ppm, while proton 21 was assigned a doublet at δ 7.15 ppm due to coupling with a neighbouring proton. Two singlets were observed for 6 protons of two methyl groups. Both of these methyl groups are in different environments. The proton at position 6 is shielded and appears upfield at δ 2.00 ppm, whereas the proton at position 8 gave a singlet at δ 2.28 ppm. The above mentioned signals are in agreement with literature.[33] The ^{13}C-NMR spectra of both series complemented the number of carbon atoms present in the members of both mono- and di-azomethine series. In both series, the most deshielded carbon signals corresponded to the characteristic imine carbon.

The total signals of NMR from this study are further compared with the literature. The signals of 4-aminoantipyrine derivatives are in good agreement with the antipyrine-based compounds reported in the literature.[34,35] The comparative analysis validates the NMR signals of the present study.

Antibacterial activity

The antibacterial activity of the synthesized compounds (**1–20**) was evaluated against *Salmonella typhi* (Gram-negative bacteria) and *Staphylococcus aureus* (Gram-positive bacteria). All the derivatives showed considerable zone of inhibition against both bacteria with ciprofloxacin taken as the standard drug. The results revealed that compound **5** and **6** exhibited excellent zones of inhibition at 51 $\pm$ 0.7 mm and 46 $\pm$ 0.5 mm, respectively against *Salmonella typhi* whereas they showed 48 $\pm$ 0.6 mm and 43 $\pm$ 0.8 mm, respectively, against *Staphylococcus*

Table 1 Zones of inhibition (mm) ± SD ($n = 3$) of mono-azomethine and di-azomethine Schiff-base derivatives of 4-aminoantipyrine against *Staphylococcus aureus* and *Salmonella typhi*[a]

Compounds	*Staphylococcus aureus* zone of inhibition (mm)	*Salmonella typhi* zone of inhibition (mm)
1	22 ± 0.3	09 ± 0.4
2	11 ± 0.8	0
3	12 ± 0.3	16 ± 0.3
4	0	13 ± 0.4
5	48 ± 0.6	51 ± 0.7
6	46 ± 0.5	45 ± 0.5
7	28 ± 1.2	19 ± 0.9
8	17 ± 0.8	18 ± 0.7
9	17 ± 1.3	10 ± 0.9
10	34 ± 0.9	25 ± 0.6
11	15 ± 0.2	0
12	14 ± 0.3	07 ± 1.1
13	38 ± 0.8	24 ± 0.7
14	11 ± 0.6	0
15	0	06 ± 0.5
16	14 ± 0.6	15 ± 0.5
17	12 ± 0.4	11 ± 0.4
18	22 ± 0.9	14 ± 0.6
19	25 ± 0.8	37 ± 0.9
20	15 ± 1.0	0
DMSO	0	0
Ciprofloxacin (standard)	62 ± 0.9	54 ± 0.5

[a] Mean ± SD ($n = 3$).

aureus as compared to the standard drug (ciprofloxacin) which showed zones of inhibition at 54 ± 0.5 mm and 62 ± 0.9 mm, respectively. The di-azomethine products were less effective, presenting zones of inhibition at 38 ± 0.8 mm with compound **13** and 34 ± 0.9 mm with compound **10** against *Staphylococcus aureu*, compound **19** showed 37 ± 0.9 mm against *Salmonella typhi*. The values of zones of inhibition of the most active compounds are summarized in Table 1.

According to the structure-activity relationship (SAR), mono-azomethine Schiff bases of 4-aminoantipyrine with –OH substitution (**5** and **6**) exhibited better anti-bacterial activity against both types of bacteria compared to di-azomethine Schiff bases (**13**, **10** and **19**). However, in both cases (mon- and di-azomethine) the compounds containing halogens were found to be the most effective in order of F > Cl > Br > I.

α-Glucosidase inhibition

All the synthesized compounds (**1–20**) were evaluated for their inhibition potential against α-glucosidase. The *In-vitro* α-glucosidase inhibition assay indicated that compound **12**, belonging to di-azomethine Schiff base series, and compound **8**, belonging to the mono-azomethine Schiff base series, exhibited excellent inhibition potential with IC_{50} values of 300 ± 22 μM and 343 ± 20 μM, as compared to standard drug acarbose with IC_{50} value of 378.2 ± 0.12 μM. Other compounds **1**, **2**, **5**, **6**, and **9** belonging to mono-azomethine Schiff bases represented inhibition with IC_{50} values in the range of 400 to 500 μM which are also comparable to the standard, as provided in Table 2.

Table 2 IC_{50} values of the most active compounds from mono-azomethine and di-azomethine Schiff bases of 4-aminoantipyrine against α-glucosidase

Compounds	IC_{50} ± SEM (μM)	Compounds	IC_{50} ± SEM (μM)
1	401 ± 11	**8**	343 ± 20
2	424 ± 14	**9**	500 ± 10
5	480 ± 08	**12**	300 ± 22
6	456 ± 12	Acarbose	378.2 ± 0.12

According to structure-activity relationship (SAR) from the data given in Table 2, compound **5** from the mono-azomethine Schiff base (IC_{50}: 480 ± 08 μM) became a more effective inhibitor when it was converted into di-azomethine Schiff base (compound **12**) with a 4-bromo substitution on the benzene ring (IC_{50}: 300 ± 22 μM). In contrast, compound **8** from the mono-azomethine with 3,5 di-methoxy substitution on the benzene ring with IC_{50} of 343 ± 20 μM was a better inhibitor compared to compound **1** and **2**, which have nitro ($-NO_2$) substitution and are more effective than compounds with others substitution on the benzene ring. This result confirms that both of the above-mentioned compounds are significantly better inhibitors of the enzyme than the standard. Therefore, it can be suggested that either any one or both of these compounds can be considered potential standard inhibitors of the enzyme. We have previously reported the α-glucosidase inhibition potential of transition metal complexes of Schiff base derivatives of 4-aminoantipyrine, showing non-competitive inhibition.[25] The remaining compounds of both series **3**, **4**, **7**, **10**, **11**, **13**, **14**, **15**, **16**, **17**, **18**, **19**, **20** showed less than 50% inhibition.

Molecular docking studies

Structure optimization

The structures of the synthesized compounds were optimized using DFT calculations in Gaussian 09, employing the B3LYP method with the 6-31G basis set.

Docking studies of the most active compound **12** with the active site of α-glucosidase (PDB ID: 1XSK) indicated that it makes a conventional hydrogen bond with Asp185 and Asp482 along with other hydrophobic interactions, having RMSD value of 1.8 Å and Gibb's free energy (S) of −9.6 kcal mol^{-1}, as shown in Fig. 3a (3D) and b (2D).

Molecular dynamic simulation

The Root Mean Square Deviation (RMSD), expressed in nanoseconds (ns), is plotted against time in this graph. In molecular dynamics simulations, RMSD is a commonly used quantity to quantify a molecule's structural divergence from a reference structure, usually its initial conformation. Greater flexibility or conformational changes are suggested by larger RMSD values, whereas lower values indicate structural stability. This plot compares two systems over a 100 ns simulation period: the complex, represented by purple, and the free protein, represented by red (Fig. 4). Within the first 10 ns, the RMSD for the free protein rapidly rises from a very low starting point of 1.5 Å. This quick increase suggests that the free protein starts to explore its structural flexibility during the first equilibration period, undergoing major conformational changes. Following this initial increase, the RMSD fluctuates during the simulation before stabilizing at 3.0 and 3.5 Å. When the free protein is not attached to any ligand, its consistently greater RMSD indicates that it is structurally flexible and explores a wider range of conformational states. Free proteins frequently exhibit this behavior because they can take on a variety of structural shapes due to the lack of connections that hold conformations in place. The complex, on the other hand, behaves very differently. Throughout the simulation, the RMSD of the complex is much lower, beginning at about 1.0 Å and stabilizing at about 1.5 Å. The complex is more stable and deviates less from its original shape, as indicated by this continuously low RMSD. The reduced fluctuations also imply that structural restrictions imposed by the interactions between the protein and its ligand limit the protein's flexibility and inhibit its ability to explore a large conformational region. Over the course of the simulation, these stabilizing interactions such as hydrophobic or hydrogen bonding help to preserve the complex structure's integrity. The stabilizing effect of the ligand in the complex is highlighted by the comparison of the two systems. The substantial variation in RMSD values between the complex and free protein highlights how ligand binding limits conformational freedom and preserves structural stability. Throughout the simulation, the complex stays comparatively rigid and stable, but the free protein shows more flexibility and structural alterations. This finding supports the widely held belief that interactions between ligands and partners frequently stabilize protein structures by locking them into functional conformations and lowering overall structural fluctuations.

The free protein has higher RMSF values all around, which suggests that its residues are more flexible and move more dynamically. Large peaks (such as those at regions ∼50, 400, and 700) indicate extremely flexible segments that could be terminal sections, unstructured loops, or other dynamic protein regions. The complex exhibits consistently lower RMSF values, which are indicative of decreased residue mobility. This implies that interactions between the protein and its ligand maintain its structure and limit the flexibility of many residues. The complex's decreased RMSF suggests that binding events stabilize the protein, particularly in flexible areas. Protein-ligand

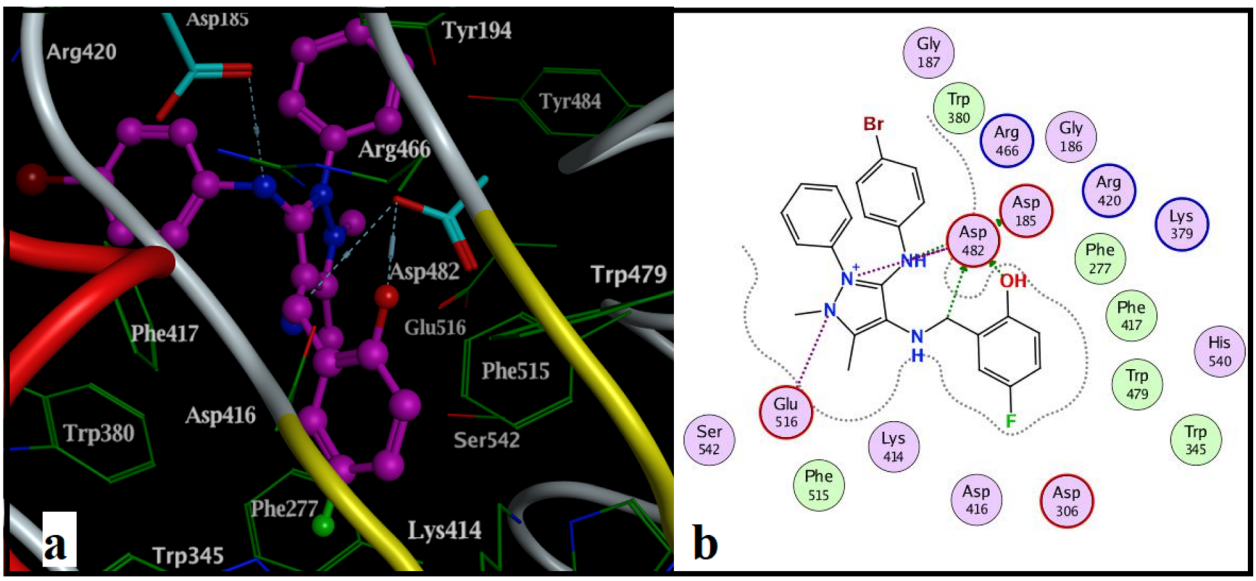

Fig. 3 (a) 3D binding pose of compound **12** (ball & stick model) with the active residues (stick model) of α-glucosidase enzyme (PDB:1XSK) in ribbon model. (b) 2D binding pose of compound **12** in the active site of enzyme representing bonds and hydrophobic interactions.

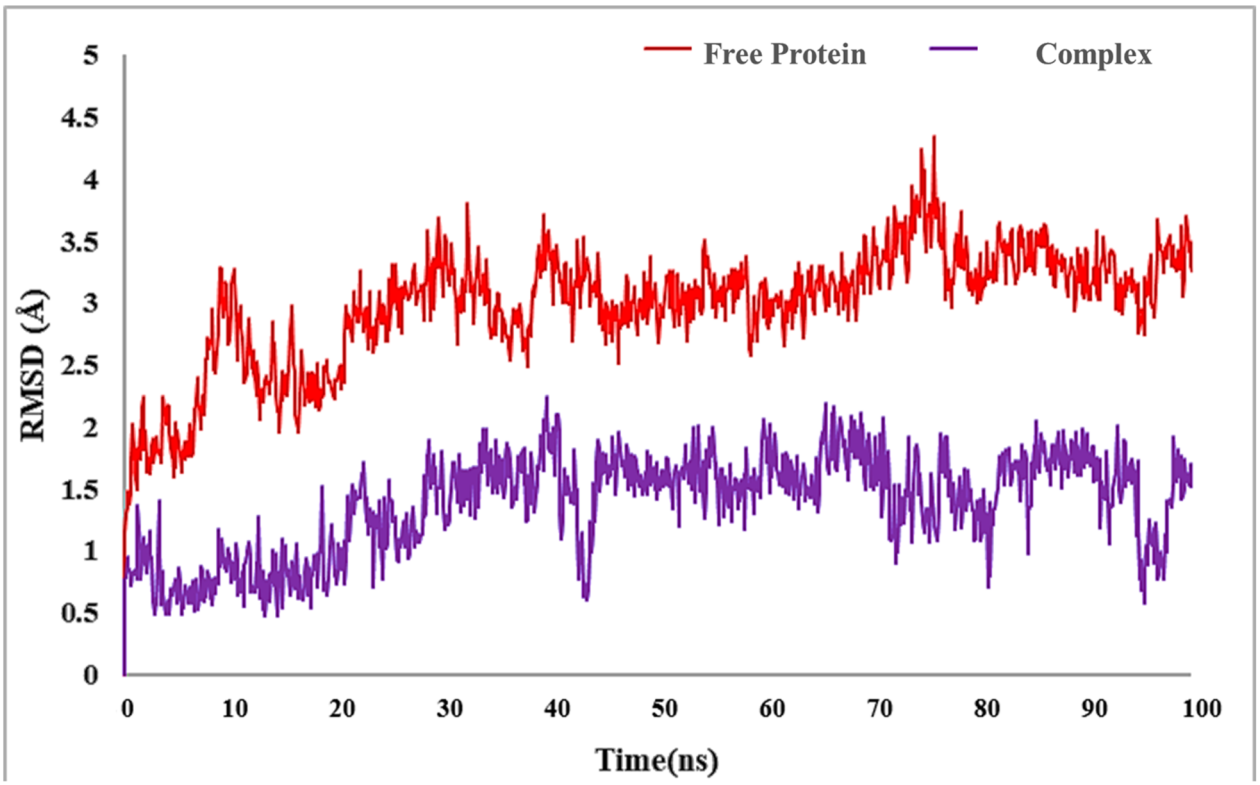

Fig. 4 RMSD trajectory analysis for protein (red colored trajectory), protein-ligand complex (purple colored trajectory).

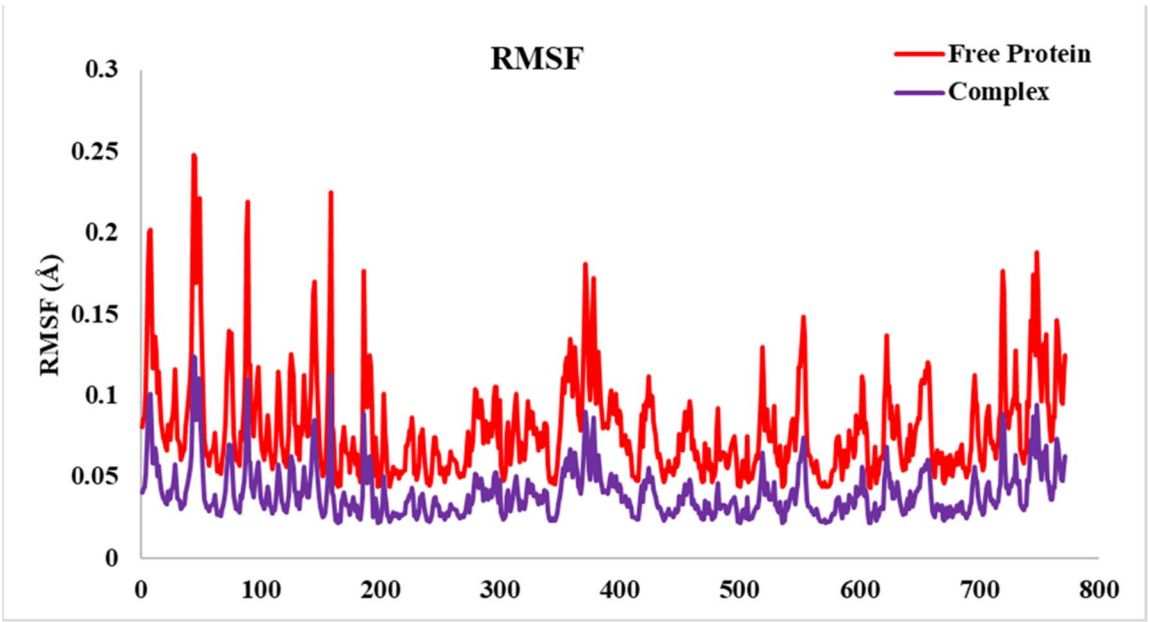

Fig. 5 RMSF trajectory analysis for protein (red colored trajectory), protein-ligand complex (purple colored trajectory).

interactions are responsible for its stabilization because they limit conformational freedom. In molecular systems where binding ligands improve structural stability, this is a typical occurrence. In conclusion, the complex is more stable, as observed by lower RMSF values, whereas the free protein is more flexible and dynamic (Fig. 5).

Conclusion

A series of new mono- and di-azomethine Schiff base derivatives of 4-aminoantipyrine were synthesized, characterized by spectroscopic techniques, and evaluated for their antibacterial activity against *Salmonella typhi* and *Staphylococcus aureus*, and enzyme

inhibition potential against α-glucosidase. Compound **5** and **6** exhibited excellent zones of inhibition at 51 ± 0.7 mm and 46 ± 0.5 mm, respectively, against *Salmonella typhi*, whereas 48 ± 0.6 mm and 43 ± 0.8 mm, respectively, against *Staphylococcus aureus* as compared to the standard drug (ciprofloxacin) which showed zones of inhibition at 54 ± 0.5 mm and 62 ± 0.9 mm, respectively. Di-azomethine Schiff bases were found to be less effective as compared to mono-azomethine molecules. The *In-vitro* α-glucosidase inhibition assay indicated that compounds **8** and **12** exhibited excellent inhibition with IC_{50} of 343 ± 20 μM and 300 ± 22 μM, respectively compared to the standard drug (acarbose) (IC_{50} = 378.2 ± 0.12 μM). Therefore, either one or both of these compounds can be considered as standard inhibitors of the enzyme. According to molecular docking studies, the most active compound **12** makes a conventional hydrogen bond with Asp185 and Asp482 as well as other hydrophobic interactions, with the active site of α-glucosidase (PDB ID: 1XSK) and is potentially important in targeting type 2 diabetes. Such enzyme inhibitors tend to introduce a delay in the absorption of carbohydrates from the digestive system and, therefore, exerts a lowering effect on postprandial blood glucose and insulin levels.

The prospect of this work is to explore further the inhibition process and determine the structure-activity relationship of the synthesized compounds for enzyme inhibition. Furthermore, other key enzymes in this cascade should also be targeted for similar studies with related molecules in order to find potent lead compounds.

Author contributions

All authors declare that they have all participated in the design, execution, and analysis of the paper and approved the final version. Anee Taj: methodology, software, formal analysis, data curation, writing – original draft. Iqra Kalsoom: methodology, software, formal analysis. Asma Zaidi: methodology, resources, software, validation. Majid Ali: methodology, software, validation, Mesaik M. Ahmed: methodology, formal analysis, Atia Masood Ahmed: methodology, resources, software, validation, S. Tasqeeruddin: writing – review & editing, project administration, funding acquisition, resources, Mohammad Zubair: resources, formal analysis, data curation. Shamina Begum: validation, software, formal analysis and writing – review & editing. Ajmal Khan: resources, formal analysis, writing – review & editing, project administration. Syed Majid Bukhari: conceptualization, supervision, resources, project administration, writing – review & editing. Ahmed Al-Harrasi: resources, formal analysis, writing – review & editing, project administration.

Conflicts of interest

The authors declare that they have no competing interests.

Data availability

The data supporting this article have been included as part of the supplementary information (SI). Supplementary information is available. See DOI: https://doi.org/10.1039/d6ra00719h.

Acknowledgements

The authors extend their appreciation to the Deanship of Research and Graduate Studies at King Khalid University, KSA, for funding this work through Small Research Group under grant number RGP.1/73/46.

References

1 M. F. E. Shehry, M. M. Ghorab, S. Y. Abbas, E. A. Fayed, S. A. Shedid and Y. A. Ammar, Quinoline derivatives bearing pyrazole moiety: Synthesis and biological evaluation as possible antibacterial and antifungal agents, *Eur. J. Med. Chem.*, 2018, **143**, 1463–1473.
2 S. A. Ibrahim, E. A. Fayed, H. F. Rizk, S. E. Desouky and A. Ragab, Hydrazonoyl bromide precursors as DHFR inhibitors for the synthesis of bis-thiazolyl pyrazole derivatives; antimicrobial activities, antibiofilm, and drug combination studies against MRSA, *Bioorg. Chem.*, 2021, **116**, 105339.
3 E. A. Fayed, S. I. Eissa, A. H. Bayoumi, N. A. Gohar, A. B. M. Mehany and Y. A. Ammar, Design, synthesis, cytotoxicity and molecular modeling studies of some novel fluorinated pyrazole-based heterocycles as anticancer and apoptosis-inducing agents, *Mol. Diversity*, 2019, **23**, 165–181.
4 E. A. Fayed, N. A. Gohar, A. H. Bayoumi and Y. A. Ammar, Novel fluorinated pyrazole-based heterocycles scaffold: cytotoxicity, in silico studies and molecular modelling targeting double mutant EGFR L858R/T790M as antiproliferative and apoptotic agents, *Med. Chem. Res.*, 2023, **32**, 369–388.
5 U. Fathy, M. N. M. Yousif, E. M. M. El-Deen and E. Fayed, Design, Synthesis, and biological evaluation of a novel series of thiazole derivatives based on pyrazoline as anticancer agents, *Egypt. J. Chem.*, 2022, **65**, 1241–1252.
6 M. Usharani, E. Akdla, R. Ashokan and R. Rajavi, Pharmacological Properties of Schiff Base Metal Complexes Derived from Substituted Pyridine and Aromatic Amine—A Review, *Int. J. Pharm. Sci. Health Care*, 2013, **5**, 1–11.
7 S. Cunha, S. M. Oliveira, J. M. T. Rodrigues, R. M. Bastos, J. Ferrari, C. M. de Oliveira, L. Kato, H. B. Napolitano, I. Vencato and C. Lariucci, Structural studies of 4-aminoantipyrine derivatives, *J. Mol. Struct.*, 2005, **752**, 32–39.
8 Y. Deswal, S. Asija, D. Kumar, D. K. Jindal, G. Chandan, V. Panwar, S. Saroya and N. Kumar, Transition metal complexes of triazole-based bioactive ligands: synthesis, spectral characterization, antimicrobial, anticancer and molecular docking studies, *Res. Chem. Intermed.*, 2022, **48**, 703–729.
9 Y. Deswal, S. Asija, A. Dubey, L. Deswal, D. Kumar, D. K. Jindal and J. Devi, Cobalt (II), nickel (II), copper (II) and zinc (II) complexes of thiadiazole based Schiff base ligands: Synthesis, structural characterization, DFT, antidiabetic and molecular docking studies, *J. Mol. Struct.*, 2022, **1253**, 132266.
10 E. A. Fayed, R. R. E. Eldin, A. B. M. Mehany, A. H. Bayoumi and Y. A. Ammar, Isatin-Schiff's base and chalcone hybrids

as chemically apoptotic inducers and EGFR inhibitors; design, synthesis, anti-proliferative activities and in silico evaluation, *J. Mol. Struct.*, 2021, **1234**, 130159.

11 A.-H. Abdel-Rahman, A. Ahmed and M. Ramiz, Synthesis and anti-hbv activity of 4-aminoanti-pyrine derivatives, *Chem. Heterocycl. Compd.*, 2010, **46**, 72–78.

12 C. Justin Dhanaraj and N. M. Sivasankaran, Synthesis, characterization, and antimicrobial studies of some Schiff-base metal (II) complexes, *J. Coord. Chem.*, 2009, **62**, 4018–4028.

13 M. El-Ajaily, R. El-Ferjani and A. Maihub, Preparation and Physical Investigation of Complexes Derived from 4-Dimethylaminobenzaldehyde and 4-Aminoantipyrine Schiff Base with Ni (II), Cu (II), Rh (III), and Pt (IV) Ions, *Jordan J. Chem.*, 2007, **2**, 287–296.

14 M. Kalanithi, M. Rajarajan and P. Tharmaraj, Spectral, biological screening, and DNA studies of metal chelates of 4-[N, N-bis-(3, 5-dimethyl-pyrazolyl-1-methyl)] aminoantipyrine, *J. Coord. Chem.*, 2011, **64**, 1436–1445.

15 N. Raman, R. S. Johnson and A. Sakthivel, Transition metal complexes with Schiff-base ligands: 4-aminoantipyrine based derivatives–a review, *J. Coord. Chem.*, 2009, **62**, 691–709.

16 L. A. Mohammed, R. T. Mehdi and A. A. M. Ali, Synthesis and Biological Screening of the Gold Complex as Anticancer and Some Transition Metal Complexes with New Heterocyclic Ligand Derived from 4-Amino Antipyrine, *Nano Biomed. Eng.*, 2018, **10**, 199–212.

17 N. El-Kholy, Synthesis, spectroscopic characterization, antimicrobial, antitumor properties of new 4-amino-2, 3 dimethyl-1-phenyl-3-pyrazolone-5-one (antipyrine) Schiff bases and its transition metal complexes, *Am. J. Sci.*, 2017, **13**, 132–145.

18 M. S. Alam and D.-U. Lee, Physicochemical analyses of a bioactive 4-aminoantipyrine analogue - synthesis, crystal structure, solid state interactions, antibacterial, conformational and docking studies, *EXCLI J.*, 2016, **26**, 614–629.

19 (*a*) E. Aguilar-Lianos, S. E. Carrera-Pacheco, R. González-Pastor, J. Zúñiga-Miranda, C. Rodríguez-Pólit, J. C. Romero-Benavides and J. Heredia-Moya, Synthesis and evaluation of biological activities of Schiff base derivatives of 4-aminoantipyrine and cinnamaldehydes, *Chem. Process.*, 2022, **12**, 43; (*b*) M. Hanefeld and G. Mertes, *Treatment: Alpha Glucosidase Inhibitors, in Encyclopedia of Endocrine Diseases*, Elsevier, 2019, pp. 238–244.

20 (*a*) A. M. Alamshany, Design, synthesis, and antimicrobial evaluation of new antipyrine derivatives bearing thiazolopyridazine and pyrazolothiazole scaffolds, *Synth. Commun.*, 2023, **54**, 22–40; (*b*) E. A. Fayed, A. Thabet, S. M. A. El-Gilil, H. M. A. Elsanhory and Y. A. Ammar, Fluorinated thiazole–thiosemicarbazones hybrids as potential PPAR-γ agonist and α-amylase, α-glucosidase antagonists: Design, synthesis, in silico ADMET and docking studies and hypoglycemic evaluation, *J. Mol. Struct.*, 2024, **1301**, 137374.

21 E. A. Fayed, R. R. E. Eldin, A. B. Mehany, A. H. Bayoumi and Y. A. Ammar, Isatin-Schiff's base and chalcone hybrids as chemically apoptotic inducers and EGFR inhibitors; design, synthesis, anti-proliferative activities and in silico evaluation, *J. Mol. Struct.*, 2021, **1234**, 130159.

22 S. M. Bukhari, R. Sarwar, A. Zaidi, M. Ali, F. A. Khan, U. Farooq and A. Al-Harrasi, Some of the organic ligand transition metal complexes can serve as potent α-glucosidase inhibitors: in-vitro, kinetics and in-silico studies, *norg. Nano-Metal Chem.*, 2023, **53**, 621–628.

23 Y. Deswal, S. Asija, A. Tufail, A. Dubey, L. Deswal, N. Kumar, S. Saroya, J. S. Kirar and N. M. Gupta, Instigating the in vitro antidiabetic activity of new tridentate Schiff base ligand appended M (II) complexes: from synthesis, structural characterization, quantum computational calculations to molecular docking, and molecular dynamics simulation studies, *Appl. Organomet. Chem.*, 2023, **37**, e7050.

24 I. Ifeanyichukwu, E. U. Eunice, I. T. Ajoko and T. T. Jim-Halliday, Molecular docking, synthesis and antimicrobial evaluation of 4-[(3-hydroxybenzalidene)amino]antipyrine and its copper complex, *Sch. Int. J. Chem. Mater. Sci.*, 2023, **6**, 149–162.

25 J. Helmersson, B. Vessby, A. Larsson and S. Basu, Association of type 2 diabetes with cyclooxygenase-mediated inflammation and oxidative stress in an elderly population, *Circ*, 2004, **109**, 1729–1734.

26 Q. Yasar and Z. Zaheer, 4-aminoantipyrine analogs as anti-inflammatory and antioxidant agents: synthesis, biological evaluation and molecular docking studies, *Int. J. Pharm. Invest.*, 2021, **11**, 14–22.

27 D. Shivakumar, J. Williams, Y. Wu, W. Damm, J. Shelley and W. Sherman, Prediction of absolute solvation free energies using molecular dynamics free energy perturbation and the OPLS force field, *J. Chem. Theory Comput.*, 2010, **6**, 1509–1519.

28 K. J. Bowers, E. Chow, H. Xu, R. O. Dror, M. P. Eastwood, B. A. Gregersen, J. L. Klepeis, I. Kolossvary, M. A. Moraes, F. D. Sacerdoti, J. K. Salmon and Y. Shan, D. E. Shaw, Scalable algorithms for molecular dynamics simulations on commodity clusters, *Proc ACM/IEEE SC, 06*, 2006, 84.

29 B. A. Luty, M. E. Davis, I. G. Tironi and W. F. V. Gunsteren, A comparison of particle-particle, particle-mesh and ewald methods for calculating electrostatic interactions in periodic molecular systems, *Mol. Simul.*, 1994, **14**, 11–20.

30 A. Hospital, J. R. Goñi, M. Orozco and J. L. Gelpí, Molecular dynamics simulations: advances and applications, *Adv. Appl. Bioinform. Chem.*, 2015, **8**, 37–47.

31 M. S. Alam and D.-U. Lee, Synthesis, molecular structure and antioxidant Activity of (E)-4-[benzylideneamino]-1,5-dimethyl-2-phenyl-1H-pyrazol-3(2H)-one, a Schiff base ligand of 4-aminoantipyrine, *J. Chem. Crystallogr.*, 2012, **42**, 93–102.

32 N. Raman, A. Kulandaisamy, C. Thangaraja, P. Manisankar, S. Viswanathan and C. Vedhi, Synthesis, structural characterisation and electrochemical and antibacterial studies of Schiff base copper complexes, *Transit. Met. Chem.*, 2004, **29**, 129–135.

33 N. Raman, A. Kulandaisamy and K. Jeyasubramanian, Synthesis, spectroscopic characterization, redox, and biological screening studies of some Schiff base transition metal (II) complexes derived from salicylidene-4-aminoantipyrine and 2-aminophenol/2-aminothiophenol, *Synth. React. Inorg. Met.-Org. Chem.*, 2001, **31**, 1249–1270.

34 M. Rocha, A. Saeed, D. M. Gil, G. A. Echeverría, O. E. Piro, A. Khurshid, M. Arshad, S. A. A. Shah and M. F. Erben, Crystal engineering with novel antipyrine derivatives: iInsights from X-ray diffraction, Hirshfeld surface analysis, and DFT calculations on intermolecular interactions, *J. Mol. Struct.*, 2025, **1319**, 139450.

35 A. Khurshid, A. Saeed, M. F. Erben, T. Hökelek and E. Jabeen, DFT guided substitution effect on azomethine reactive center in newly synthesized Schiff base aromatic scaffolds; syntheses, characterization, single crystal XRD, Hirshfeld surface and crystal void analyses, *J. Mol. Struct.*, 2023, **1273**, 134215.